Integrated structural health assessment using piezoelectric active sensors

Jeannette R. Wait, Gyuhae Park* and Charles R. Farrar
Engineering Sciences & Applications, Weapon Response Group, Los Alamos National Laboratory, Los Alamos, NM 87545, USA

Abstract. This paper illustrates an integrated approach for identifying structural damage. The method presented utilizes piezoelectric (PZT) materials to actuate/sense the dynamic response of the structures. Two damage identification techniques are integrated in this study, including impedance methods and Lamb wave propagations. The impedance method monitors the variations in structural mechanical impedance, which is coupled with the electrical impedance of the PZT patch. In Lamb wave propagations, one PZT patch acting as an actuator launches an elastic wave through the structure, and responses are measured by an array of PZT sensors. The changes in both wave attenuation and reflection are used to detect and locate the damage. Both the Lamb wave and impedance methods operate in high frequency ranges at which there are measurable changes in structural responses even for incipient damage such as small cracks, debonding, or loose connections. The combination of the local impedance method with the wave propagation based approach allows a better characterization of the system's structural integrity. The paper concludes with experimental results to demonstrate the feasibility of this integrated active sensing technology.

1. Introduction

Piezoelectric materials, such as Lead Zirconate Titanate (PZT), are very useful in structural health monitoring because they can perform both duties of sensing and actuation within a local area of the structure. The molecular structure of PZT materials produces a coupling between the electrical and mechanical domains. This type of material generates mechanical strain in response to an applied electric field. Conversely, the materials produce electric charges when stressed mechanically. This coupling property allows one to design and deploy an "*active*" and "*local*" sensing system whereby the structure in question is locally excited by a known input, and the corresponding responses are measured by the same excitation source. Some advantages of these devices are: compactness, light-weight, low-power consumption, ease of integration into critical structural areas, ease of activation through electrical signals, higher operating frequency, and low cost. The employment of a known input also facilitates subsequent signal processing of the measured output data. Examples of documented success using PZT materials in the areas of active and local sensing are Lamb wave propagations [1,2] and the impedance-based structural health monitoring methods [3], which are the subjects of this paper.

This paper illustrates damage identification processes in structures based on both self-sensing impedance methods and Lamb wave propagation methods. In particular, the impedance method has been used for detecting joint connection damage and the Lamb wave propagation method has been used for identifying surface cracks. The integration procedure of these two techniques is straightforward because the same PZT patches can be used for both methods. The combination of the local impedance method with the wave propagation based approach allows a better

*Corresponding author: Gyuhae Park, Ph.D., Engineering Sciences & Applications Division, Mail Stop T001, Los Alamos National Laboratory, Los Alamos, NM 87545, USA. Tel.: +1 505 663 5335; Fax: +1 505 663 5225; E-mail: gpark@lanl.gov.

characterization of the system's structural integrity. The coupling of these two approaches also makes the damage identification process more redundant such that the loss of a particular patch does not render the health monitoring system nonfunctional. The principle behind these two methods, experimental procedures and results, and additional issues that can be used as a guideline for future investigations are presented in the following sections.

2. Methodology

2.1. Impedance method

The impedance-based monitoring technique uses both the direct and converse version of the piezoelectric effect simultaneously to obtain an impedance signature for the structure. When a PZT patch is driven by a fixed, alternating electric field, a small deformation is produced in the PZT wafer and the attached structure. The subsequent structural response to the mechanical vibration is transferred back to the PZT wafer in the form of an electrical response. When damage causes the mechanical dynamic response to change, it is manifested in the electrical response of the PZT wafer. The electrical impedance, which is the ratio of the input voltage to the output current, is related to the structural impedance through the following equation [4]:

$$Y(\omega) = \frac{I}{V} = i\omega a \left(\varepsilon_{33}^T - \frac{Z_s(\omega)}{Z_s(\omega) + Z_a(\omega)} d_{3x}^2 \hat{Y}_{xx}^E \right) \tag{1}$$

In Eq. (1), Y is the electrical admittance (inverse of impedance), Z_a and Z_s are the PZT patch's and the structure's mechanical impedances, respectively, Y_{xx}^E is the complex Young's modulus of the PZT patch under zero electric field, d_{3x} is the piezoelectric coupling constant in the arbitrary x direction at zero stress, ε_{33}^T is the dielectric constant at zero stress, a is a geometric constant of the PZT patch, and ω is the angular frequency. When a structure is damaged, the mechanical impedance is altered by changes in the structural mass, stiffness, and/or damping. Because all other variables in Eq. (1) are determined by the PZT properties, only the external structure's impedance, Z_s, uniquely determines the overall electrical impedance of the PZT patch. Therefore, a change in the electrical impedance is regarded as an indication that the structure has been damaged. The impedance-based method is shown to be excellent at localizing damage because inputs to the structure is generally greater than 30 kHz, which limits the dynamic response of the structure to the local area of the PZT patch. For more information on current impedance-based structural health monitoring (SHM) methods, consult [3,5–9].

The impedance method has been previously integrated with model-based damage identification techniques. Park et al. [10] combined the impedance method with a model-based damage identification technique for 1-D structures. Once the location of damage was identified with the impedance method, the frequency response function data measured by the same PZT patch was utilized to characterize structural damage. Naidu et al. [11] utilize the changes in the resonant frequencies of a structure, which is measured by the impedance signature, to identify the locations of structural damage. The integration of the impedance method and the wave propagation approaches was also investigated by Giurgiutiu et al. [6]. A simple geometry was used to analyze the pulse-echo technique and changes in wave phase and velocity were used to identify locations of damage. They conclude that while the impedance-based approach is more suitable for near-field damage detection, the wave propagation based approach is more applicable for far-field damage detection.

The integration scheme proposed in this paper, however, is different from the previous approaches. The impedance method is to monitor the joint connection damage, and the Lamb wave propagations are primarily used to monitor surface and crack formations, because we found that each method is more sensitive to specific damage, as described in the next sections.

2.2. Lamb wave propagations

Since the 1960s, the ultrasonic research community has studied Lamb waves for the nondestructive evaluation of plates [12]. Lamb waves are mechanical waves corresponding to vibration modes of plates with a thickness on the same order of magnitude as their wavelength. The advances in sensor and hardware technologies for efficient

generation and detection of Lamb waves and the need to detect sub-surface damage in laminate composite structures has led to a significant increase in the use of Lamb waves for detecting defects in structures.

The dispersive nature of Lamb waves means that the different frequency components of the Lamb waves travel at different speeds and that the shape of the wave packet changes as it propagates through solid media. There are two types of modes that form in a plate when excited with Lamb waves: asymmetric (A) and symmetric (S). The asymmetrical modes are analogous to shear waves (equivalent to S waves in earthquake engineering), while symmetrical modes are analogous to compression waves (equivalent to P waves in earthquake engineering). The selection of the excitation frequency for Lamb waves must be made so as to excite a structure at a certain mode (S_0 or A_0) and to avoid any higher modes that might also be present. Lamb wave propagation methods look for the possibility of damage by tracking changes in transmission velocity and wave attenuation/reflections. Several methods have been proposed to enhance the interpretation of the measured Lamb wave signals to detect and locate structural damage. They are based on changes in wave attenuations using wavelets [1,13], time-frequency analysis [2], wave reflections, and time of flight information [1,6,14]. A more complete description on the Lamb wave propagation technique can be found in the references [1,12].

3. Test structures & experimental results

Two structures were tested to investigate the feasibility of using impedance-based methods and Lamb wave propagations to detect varying types and degrees of damage. Each structure was instrumented with PZT actuators/sensors. A simulated three-story building was first used to demonstrate the effectiveness of the impedance method in detecting and locating connection damage in a structure. A built-in aluminum cantilever plate is then used to illustrate how the two active sensing techniques (impedance-based and Lamb wave) can be integrated together using the same PZT sensor/actuator.

3.1. Scaled 3-story building structure

Description of structure

The simulated three-story building structure, Fig. 1, is constructed of aluminum unistrut columns and aluminum floor plates. Floors are 1.3-cm-thick aluminum plates with two bolt connections to brackets on the unistrut columns. The base is a 3.8-cm-thick aluminum plate. Support brackets for the columns are bolted to this plate. All bolted connections are tightened to a torque of 12.4-Nm for the undamaged state. Four Firestone air mount isolators, which allowed the structure to move freely in horizontal directions, are bolted to the bottom of the base plate. The isolators are inflated to 140-kPa.

Four PSI-5A PZT patches (2.5-cm × 2.5-cm × 0.025-cm) are bonded to the brackets that affix the second floor to the unistrut columns for acquiring electrical impedances, as shown in Fig. 2. Theses PZT patches are bonded directly to the surface using a high-strength adhesive to ensure a better mechanical interaction. The PZT actuators/sensors are non-intrusive to the structure because of their small size. The impedance measurements are made through an Agilent 4294A impedance analyzer in the frequency range of 125–135 kHz. The frequency range for a given structure is usually determined by a trial and error method. It has been found that a frequency range with a high mode density exhibits a higher sensitivity, because it generally covers more structural dynamic information [3]. This selected frequency range shows the good dynamic interaction from the all four PZT patches. After measuring several baseline impedance signatures, damage is introduced by loosening one bolt at selected locations. Two damage conditions are imposed on this structure in sequence, as follows.

– Damage I: loosening a bolt at Joint 2.
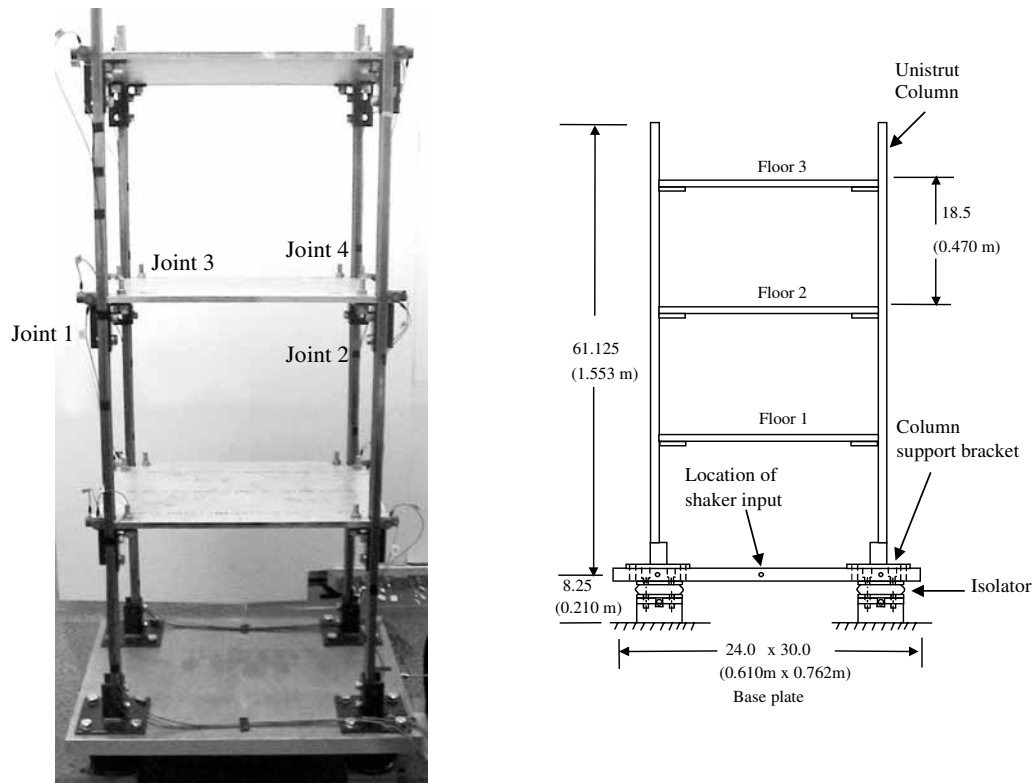– Damage II: loosening a bolt at Joint 3.

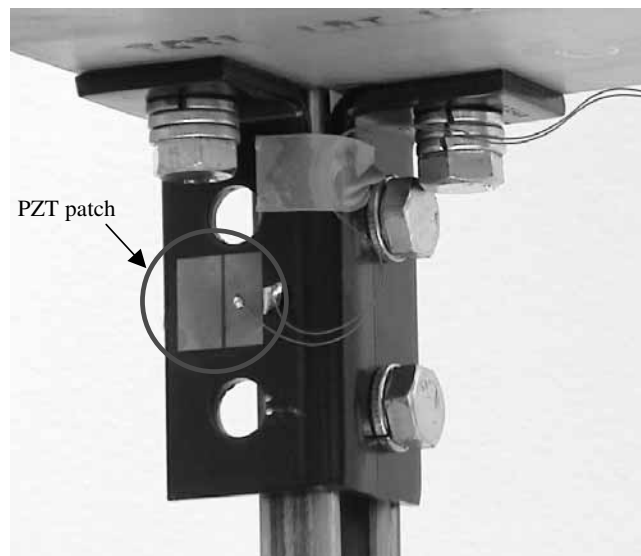Fig. 1. Scaled Model of a 3-Story Building Structure.

Fig. 2. Close-up of Joint 3 with PZT patch bonded to Bracket.

Damage interrogation and experimental results

The impedance measurements (real part) of the PZT patch at Joint 2 under the first damage condition (Damage I) are shown in the Fig. 3. When damage is induced, a significant change occurs in the signature pattern of the impedance curve over the entire frequency range from the PZT patch installed on the damaged joint. This is because
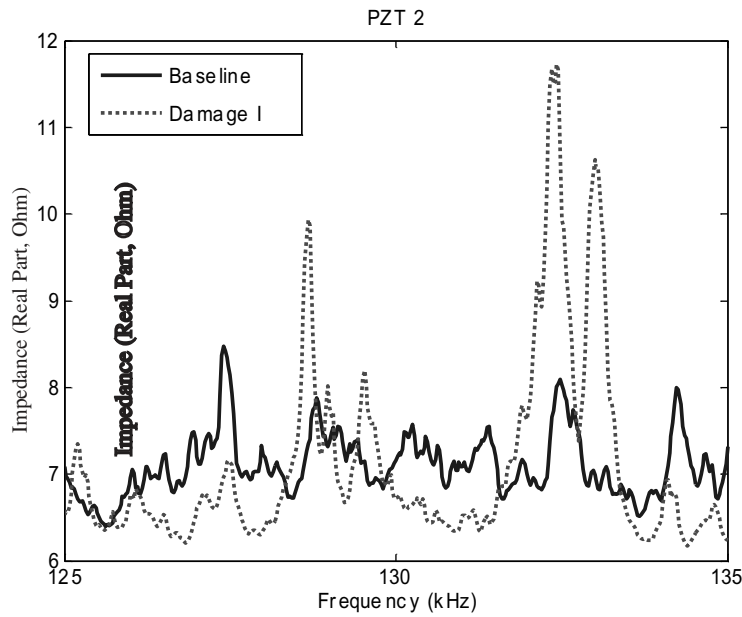
PZT 2

Fig. 3. Electrical Impedance measurement from PZT 2 before and after Damage I.
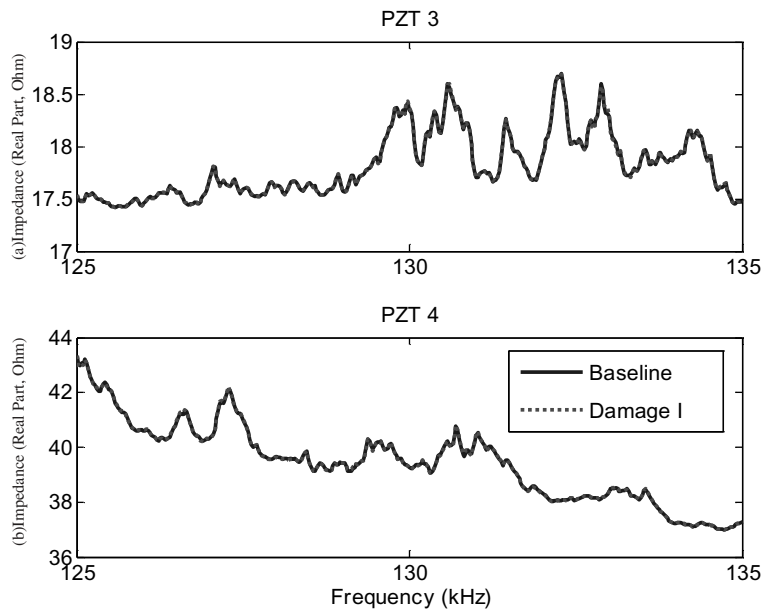
PZT 3

PZT 4

Fig. 4. Electrical Impedance measurement from PZT 3 and PZT 4 before and after Damage I.

the damage causes changes in stiffness or damping of the joint resulting in changes in mechanical impedance of the joint. The measurements taken from the PZT sensors bonded on Joints 3 and 4 do not show any changes, as shown in Fig. 4. No variations occur in these signatures because Damage I is well out of the sensing range of these PZT patches. As illustrated in this example, the impedance responses from PZT patches are extremely sensitive to any damage occurring in the near-field and are not affected by far-field damage. Therefore, by monitoring the impedance variations of each sensor, the damaged connection can be detected and located with confidence.

The same results have been observed under Damage II as is illustrated in Figs 5 and 6. A complete change occurs
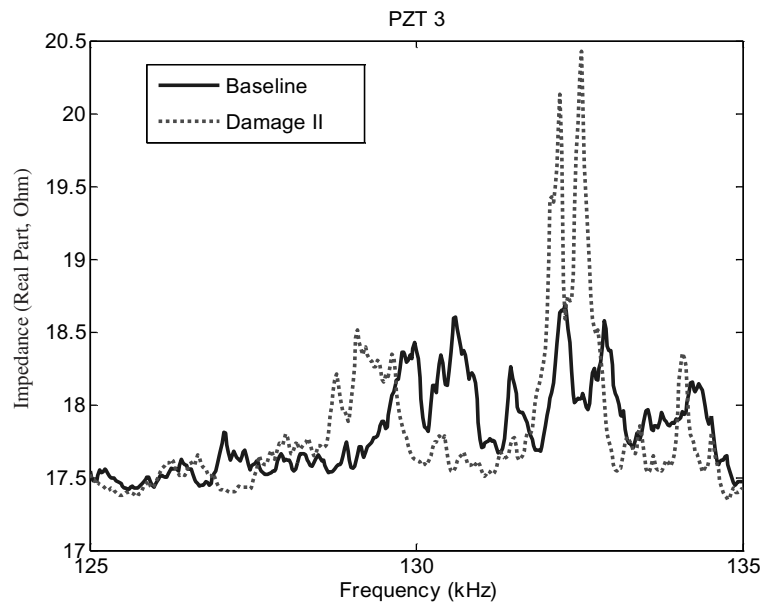
Fig. 5. Electrical Impedance measurement from PZT 3 before and after Damage II.

in the signature pattern of the curve over the entire frequency range when the damage is introduced close to the sensor location. If damage is distant (at another joint), there are only minor variations of the existing signature pattern. This limited sensing area also helps to isolate the effect of damage on the signature from other far-field changes such as mass-loading, or environmental and boundary conditions. The structure has been tested using several vibration-based methods to detect and locate connection damage [15,16]. Previous studies, however, did not efficiently locate the damaged connection relying on the lower-order global responses. As shown in this example, the impedance method provides a practical means to detect and locate structural damage with much lower hardware requirement and computational process.

3.2. Cantilever aluminum plate structure

Description of structure

The aluminum plate, shown in Fig. 7, is 101.5-cm × 10-cm × 3-mm-thick. Four holes, 1.35-cm in diameter, at one end of the plate allow it to be bolted, in a cantilevered condition, to two steel angles in 10.5-cm × 6.5-cm × 6.35-mm-thick. These angles are again jointed into 20.32-cm-long unistrut columns. The unistrut columns are bolted to an aluminum base plate (38-cm × 14-cm × 1.4-cm) and all bolted connections are tightened to a torque of 16.9-Nm for all tests.

The cantilevered aluminum plate is instrumented with four PSI-5A PZT patches and two Macro-Fiber Composite (MFC) patches. The MFC patches are a relatively new type of piezoelectric actuators that are more flexible than the conventional PZT patches. The locations and the numbering schemes of these actuators/sensors are also shown in Fig. 7. Both the impedance method and the Lamb wave propagation techniques are used to interrogate this structure using the combined network of PZT and MFC patches. Ideally, only three patches (P4, M1, M2) are required for the Lamb wave propagation analysis. However, because of equipment limitations, i.e. the same PZT patch cannot be used as a sensor and an actuator simultaneously; another PZT (or MFC) wafer is installed directly beside a PZT (or MFC) patch, to measure wave reflections that occur at the actuation location.

Lamb wave propagation method
Description of Damage cases

Several damage cases are investigated with the Lamb wave method for the aluminum plate. Simulated damage is introduced to the cantilevered plate by clamping a pair of small blocks (4-cm × 1.5-cm × 1.5-cm) to the plate with
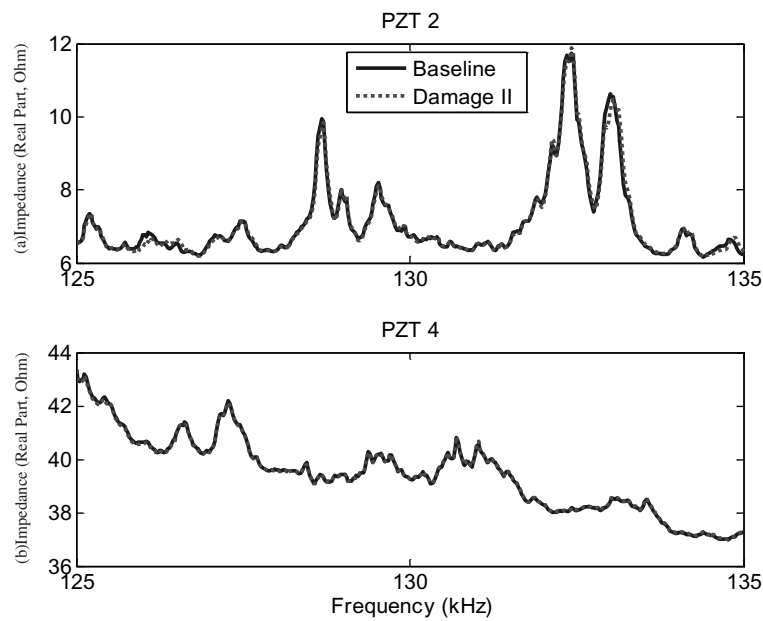
Fig. 6. Electrical Impedance measurement from PZT 2 and PZT 4 before and after Damage II.
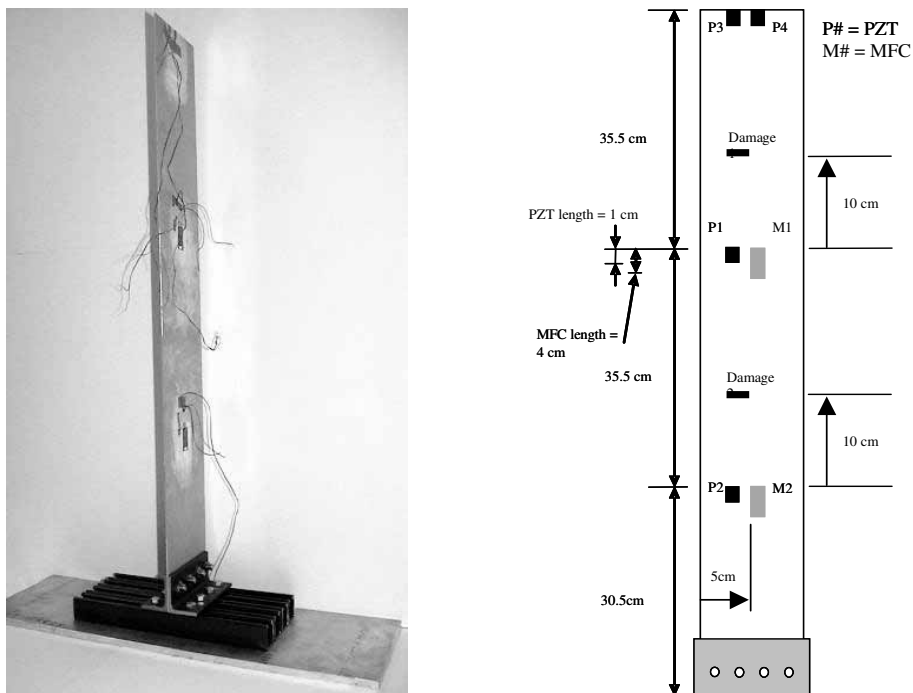

Fig. 7. Cantilevered Aluminum Plate. PZT and MFC patches are mounted at 3 Locations.

a c-clamp (one block on the front side of the plate and one on the back side of the plate). Clamping the blocks to the plate simulates changes in the flexural/extensional stiffness and the inertia of the plate in a localized area, similar to the effects of crack formation. Although clamping the blocks to the plate does not represent "real" damage, the process allows multiple tests to be performed with several different configurations. Two of the results for the
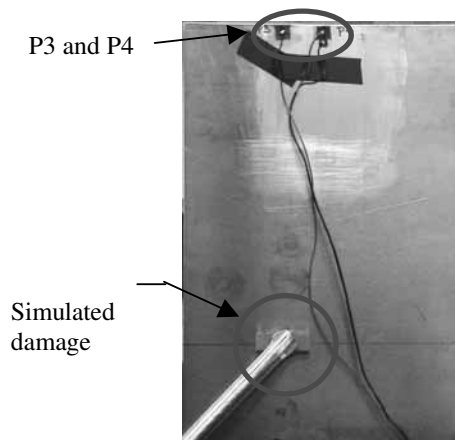
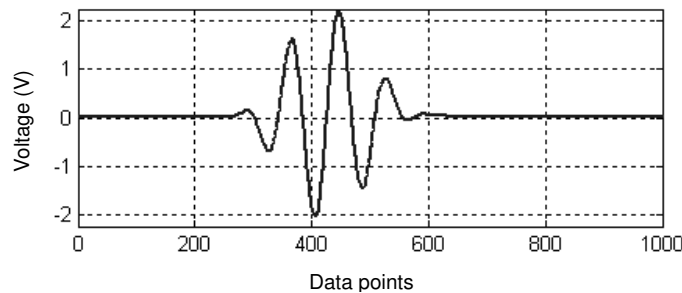Fig. 8. Damage I (between P1 and P3) introduced to the Plate, as a simulated crack.

Fig. 9. Lamb wave input excitation at 300 kHz.

simulated crack damage cases are presented here:

– Damage 1: simulated damage between P3 and P1.
– Damage 2: simulated damage between P1 and P2.

Figure 7 also shows the location of damage 1 and 2. The first damage case, introduced between P3 and P1 (Damage 1), is shown in Fig. 8. Then, for the second damage case, the pair of blocks is placed between P1 and P2. Before the simulated damage is initiated in the plate, several baseline data sets for all actuator-sensor pairs are acquired in order to establish undamaged threshold limits. Then, the same date sets are collected for each damage case. Each data set for all actuator-sensor pairs (baseline and damage cases) is repeated five times.

Analysis & Results

As was stated in Section 2.2, the selection of the input excitation for Lamb waves is very important. Care must be taken to design the most appropriate input to obtain useful results from the Lamb wave analyses. There are several factors that need to be considered when designing the input Lamb wave such as frequency and shape of the signal. The method that was used to design the input Lamb wave for this test can be found in [1]. For the tests performed on the cantilevered aluminum plate, the optimal input Lamb wave is a 300-kHz windowed sine function with four cycles (see Fig. 9). The Lamb wave measurements are made through an SMART suitcase from Acellent Technology.

For damage identification, the wave attenuation feature is first used to locate the region of the suspected damaged area, and then, the pulse-echo analysis (wave reflections) is used to locate the damage site. The principle of the pulse-echo analysis is that the damage (or discontinuity) produces diffracted waves, referred to as "a mode conversion process" [17], which creates new (reflected) waves depending on the angle of incidence. Both S_0 and A_0 modes can be created by this process. In this study, only the reflected S_0 modes are tracked because they travel much faster than the A_0 mode.
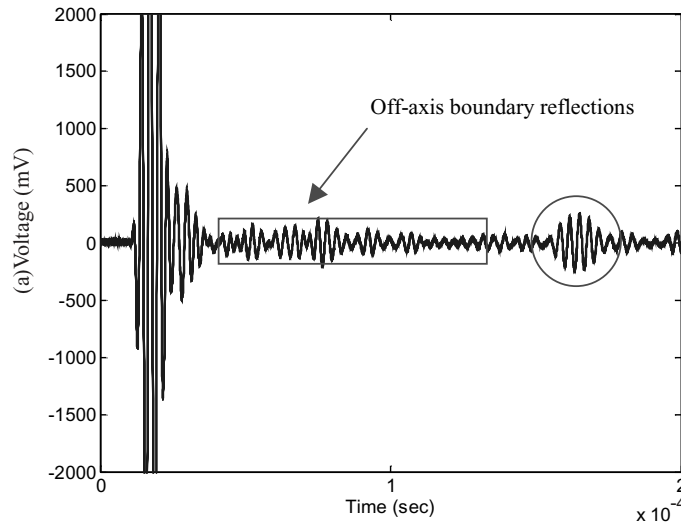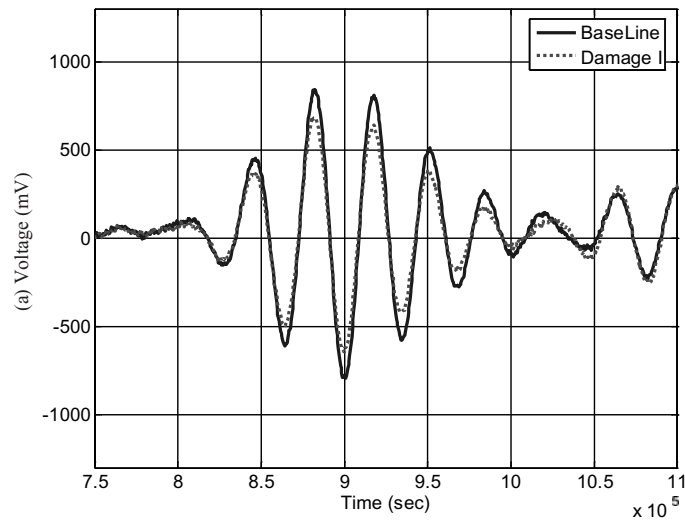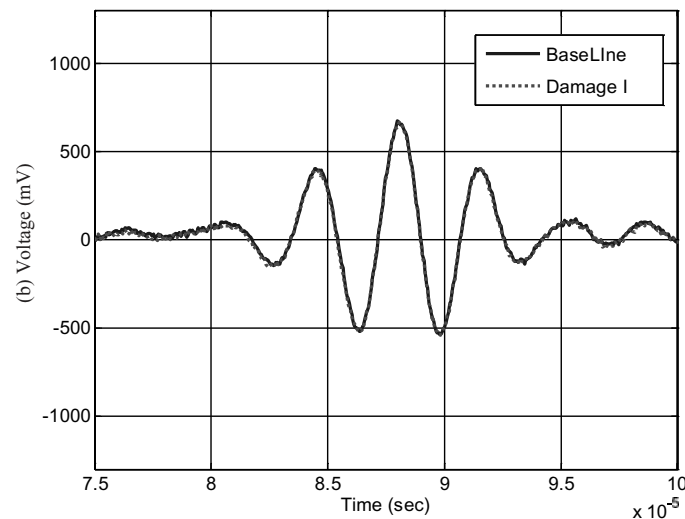
(a) M1 Sensor Response to Actuation by P1
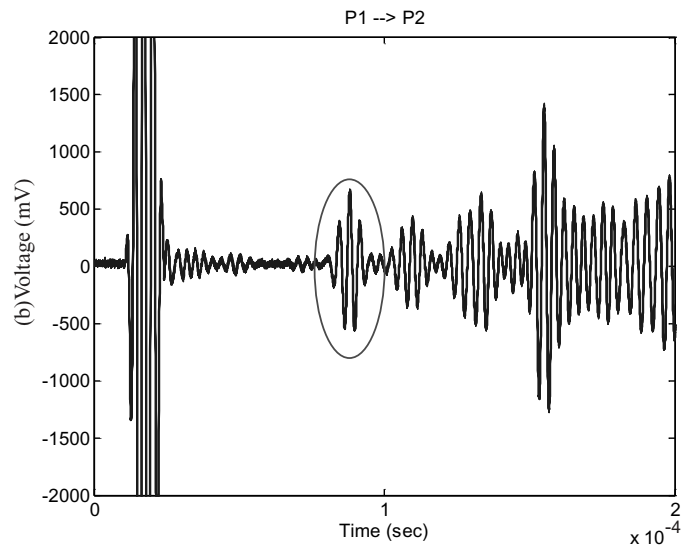
(b) P2 Sensor Response to Actuation by P1

Fig. 10. Baseline Measurements from Different Actuator-Sensor Pairs (red circles indicated first arrival of S_0 mode) (a) M1 Sensor Response to Actuation by P1; (b) P2 Sensor Response to Actuation by P1.

The Lamb wave propagations of ten baselines, with P1 as an actuator and M1 as a sensor (which can be considered as co-location), and the actuator-sensor pair of P1 and P2, with the first arrival of the S_0 mode, are shown in Fig. 10. Only one out of five measurements is shown. The group velocity for both S_0 and A_0 is measured to be approximately 5-m/ms, and 3.4-m/ms respectively. These velocities are measured between P1 and P2 and are close to the analytical prediction available in the literature. Because of the relatively small size of the structure, the reflected waves from the boundaries are measured in the sensor responses, which makes the pulse-echo analysis quite difficult. The reflections come mainly from the boundaries, which are perpendicular to the wave path. The MFC patches were used to alleviate the problem associated with the boundary reflection because of their unidirectional sensing capability. However, as can be seen in the Fig. 10, the MFC patch can still measure the waves coming from the vertical direction with
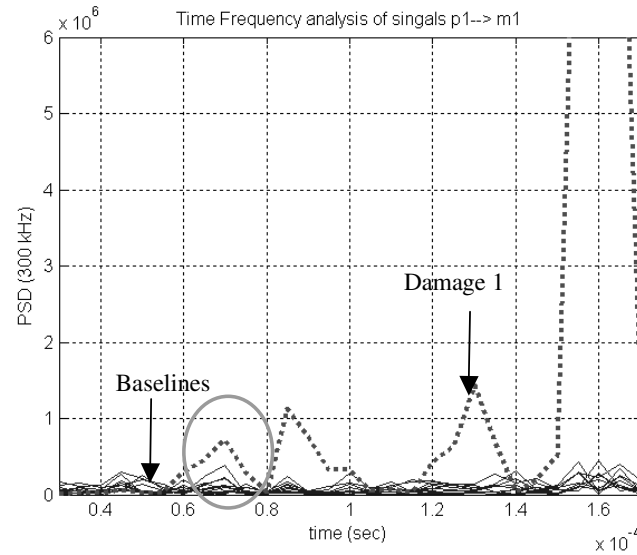
(a) P3 Sensor Response to Actuation by P1

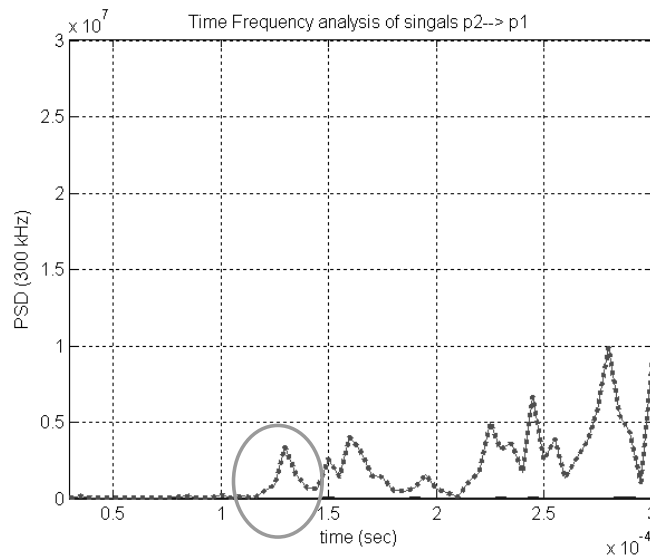(b) P2 Sensor Response to Actuation by P1

Fig. 11. The First arrival of A_0 modes (a) P3 Sensor Response to Actuation by P1; (b) P2 Sensor Response to Actuation by P1.

a somewhat distorted shape. The problem associated with the boundary-reflected waves becomes more significant, if the boundary-reflected waves are out-of-phase with the damage-reflected waves, the result is attenuation instead of increased amplitude in the combined measured reflected waves. Therefore, in this analysis, the first occurrence of changes in waves (of both attenuation and increase in amplitude) is considered as a damage indication. This is based on the assumption that there always exists the direct wave path between the damage (simulated crack) and the actuator.

As a first step for the location of damage for cases 1 and 2, the wave attenuation between P1 and P3, P1 and P2, and between P2 and the clamped boundary are recorded. The changes in each path are considered as the presence of damage in the corresponding region. Once the damaged region is identified, the location of the simulated damage is inversely identified by tracking the time of flight of the reflected wave from the actuator location, similar to processes used for triangulation procedures. For damage 1, there is large attenuation in the path between P1 and P3, while

(a) M1 Sensor Response to Actuation by P1

(b) P2 Sensor Response to Actuation by P1

Fig. 12. Time-Frequency Analysis (300 kHz). First reflection indicated in circles (a) M1 Sensor Response to Actuation by P1; (b) P2 Sensor Response to Actuation by P1.

no changes are observed in any other actuator-sensor pairs. This result indicates that the region between P1 and P3 contains the damage, as shown in Figs 11 (a) and (b). Once the damaged region is identified, the pulse-echo analysis is performed to locate the damage site. For this process, a time-frequency analysis was performed on baseline and damage cases. Analyzing time and frequency components simultaneously produces a clearer indication of the arrival of the reflected waves. In the time-frequency analysis, changes in the power spectral density (PSD) corresponding to 300 kHz, which is the frequency of the input Lamb wave, are recorded as a function of time. The PSD is defined as the amount of power per unit of frequency as a function of the frequency. Mathematically, it is defined as the Fourier transform of the autocorrelation sequence of the time series. The magnitude of the algebraic difference between the test and baseline PSDs are processed with the time-frequency analysis.
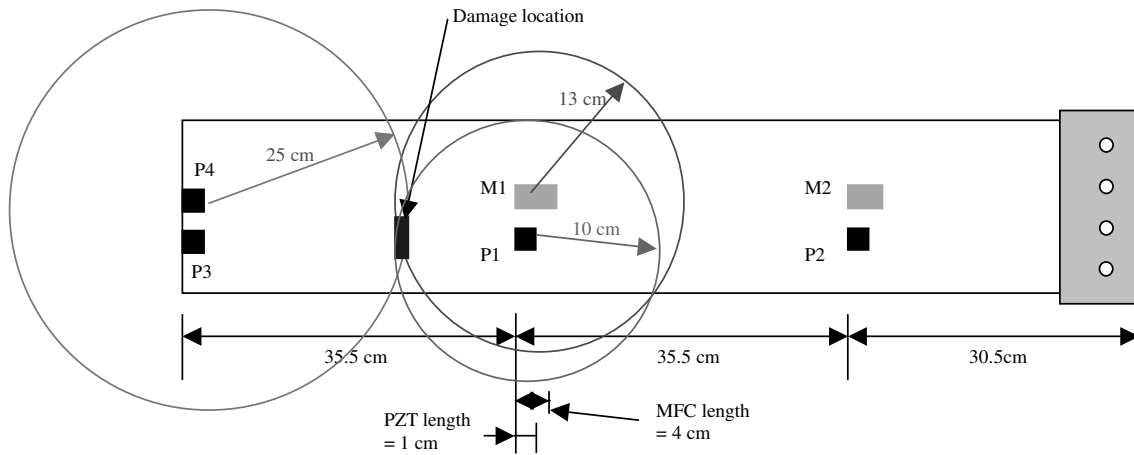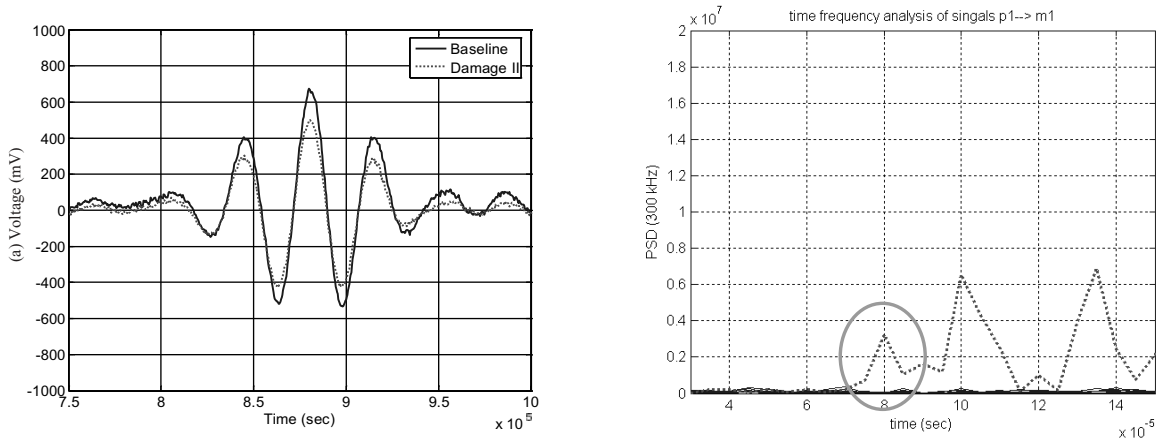
Fig. 13. Damage Location Process for Damage I.

When there are changes to the host structure's material and geometric properties, such as a surface crack or wall-thinning caused by corrosion, a portion of the Lamb wave will be reflected from the damaged location back to the sensors. This reflection can be used to locate the damage site by measuring how long damage reflected wave travels (time of flight). The first arrival of the reflected wave causes a change in the magnitude of the PSD. As can be seen in Fig. 12(a), the first reflected wave for the actuator-sensor pair, P1 and M1 (co-location), occurs at 5.5×10^{-5} seconds (the actuation was initiated at 1×10^{-5}-seconds), which indicates that the damage is located around 0.13-m ($(5.5 \times 10^{-5}$-seconds/2$) \times 5 \times 10^3$-m/s) from the sensor. Another analysis is performed for the P2 and P1 combination (distance from sensor = $[(1.3 \times 10^{-4}$-sec $- 0.8 \times 10^{-4}$-sec)/2$] \times 5 \times 10^3$-m/s = 0.10-m), as shown in Fig. 12(b) and for the path between P3 and P4 d = 0.25-m. From these three actuator-sensor pairs, the damage case 1 is located using a modified triangularization procedure (see Fig. 13).

Similar results were observed in Damage 2. The first arrival of the S_0 mode shows a significant attenuation in the region between P1 and P2. Again, the suspected area is identified by using time-frequency analysis of each path. Once the damage region was identified, the P1-M1 and P2-M2 combination was used to pinpoint the location of damage. Figure 14 shows the wave attenuation, time-frequency analysis, and damage localization process for damage 2.

In most cases, the detection and localization of damage was successful. However, there are a few cases that the proposed method fails to locate damage. First, if the damage is located too close to the sensor/actuator, the reflected waves are easily mixed with the (electromagnetic) actuation signals and make the damage localization difficult. In addition, if the blocks (simulated damage) are placed parallel to the length of the plate and the wave propagation path, only a little attenuation is produced. Furthermore, the existence of the boundary reflected waves makes it complicated to identify and to distinguish the "damage" reflected waves. Ideally, the pulse-echo analysis should be performed before the first boundary reflected wave arrives back at the actuator. Nevertheless, the combined use of the features associated with wave attenuation and reflection enables the detection and location of damage with fewer sensors/actuator combinations compared to methods based on only one feature. The advantage will be more significant, if the method is combined with the impedance methods for the crack identification process, because the impedance method is most sensitive to the near-field damage, and not affected by any changes that occur in the far-field.

It should be noted that the impedance analysis was not performed for Damage 1 and 2 because of the relatively large mass (weight of blocks and C-clamp) induced by the simulated damage. Preliminary experiments show that there were distinct changes observed in the impedance signatures before and after the simulated damage, but the changes may not be solely caused by the simulated damage. The change in the signatures is most likely influenced by the relatively large weight of the C-clamp. Actual, physical, surface cracks will be introduced in future experiments and the impedance method will then be used to assess the condition of the test structure. There is, however, ample evidence that the impedance methods can detect and locate surface damage by tracking the high frequency impedance

(a) P2 Sensor Response to Actuation by P1

(b) M1 Sensor Response to Actuation by P1
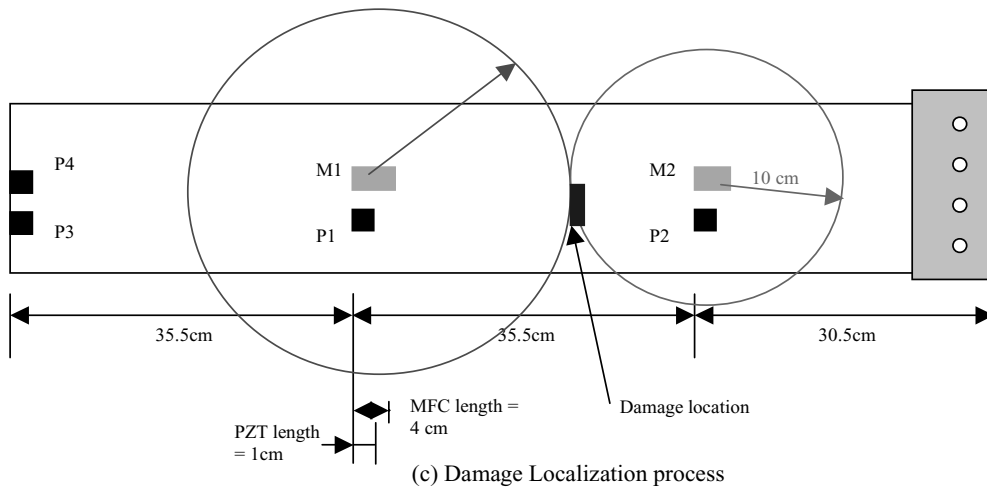
(c) Damage Localization process

Fig. 14. Damage Localization process for Damage II (a) P2 Sensor Response to Actuation by P1; (b) M1 Sensor Response to Actuation by P1; (c) Damage Localization process.

changes [3]. Instead, in this study, the impedance method is used to identify the connection damage only at the clamped-end. Damage is introduced by loosening one of the bolts through the two steel angles. As will be illustrated next, the impedance method shows the extreme sensitivity to joint-connection damage, while the Lamb wave method does not show any comparable performances.

Impedance method

Description of Damage cases

The next experiments include identifying connection damage using impedance methods. This type of damage is introduced by loosening one of the connection bolts in the clamped end of the test structure. The impedance (real part) of P2, in the frequency range of 100–105 kHz, is shown in Fig. 15 with two different damage conditions. Only the real portion of the electrical impedance is analyzed to predict damage because it is more sensitive to structural changes than the imaginary part. For the first damage case, Damage A, the bolt torque is reduced to 8.5-Nm from 16.9-Nm. Damage B refers to the condition where the same bolt has been loosened to 1.1-Nm.

Analysis & Results
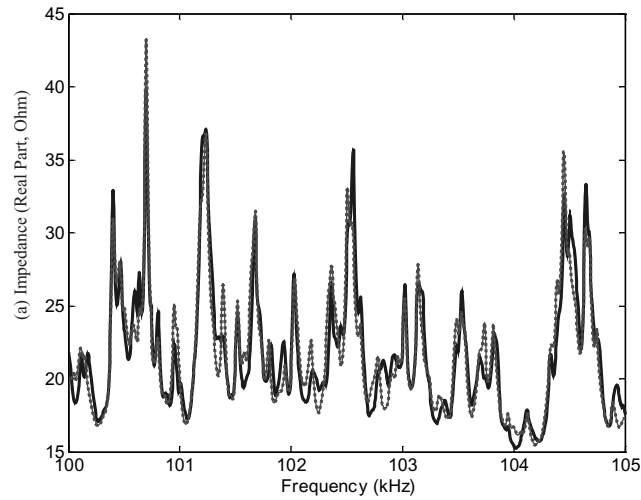
(a) Damage A (8.5-Nm)
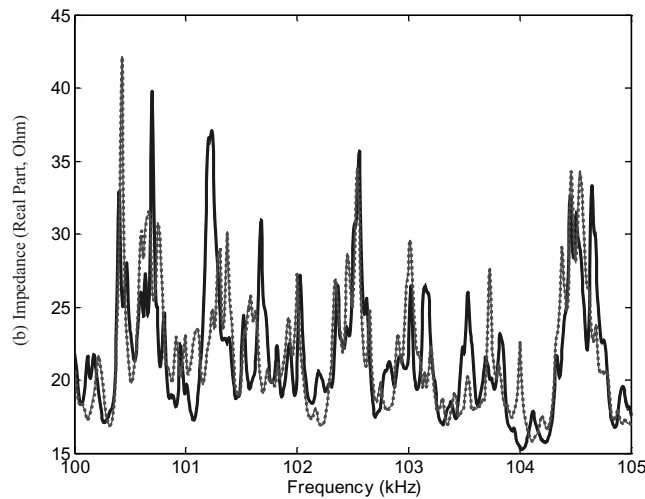
(b) Damage B (1.1-Nm)

Fig. 15. The Impedance (Real Part) Measurement for P2 for Two Connection-type Damage Cases (Solid Line: Baselines, Dotted line: Damage) (a) Damage 1 (8.5-Nm); (b) Damage 1 (1.1-Nm).

It can be seen from the impedance signatures in Figs 15(a) and (b) that, with an increasing level of damage, the impedance signature shows a relatively large change in shape and it clearly indicates imminent damage. For the first level of damage, only a small variation along the original signal (undamaged curve) is observed. This is because the first level of damage can be categorized as the incipient stage. When the bolt is loosened to a torque of 1.1-Nm, the impedance signature shows more pronounced variations as compared to previous readings; i.e. new peaks and valleys appear in the entire frequency range. This variation occurs because the loosened bolt modifies the apparent stiffness and damping of the joint. This large disparity shows the extreme sensitivity of the impedance-based method to the presence of connection-type damage in the structure.

A damage metric chart is illustrated in Fig. 16 for both Damage A and B. In this analysis, correlation coefficients are used to compare the baselines and damage test cases. The correlation determines the linear relationship between the two data sets,
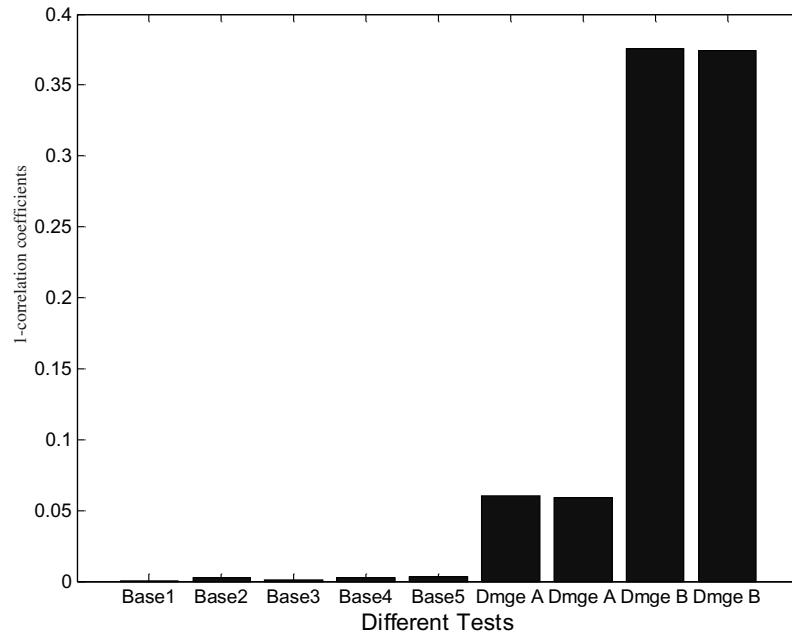
Fig. 16. Cross Correlation Damage Metric Chart.

$$\rho = \frac{(\text{Re}(Z_{i,1}) - \text{Re}(Z_1))(\text{Re}(Z_{i,2}) - \text{Re}(Z_2)}{\sigma_{z_1}\sigma_{z_2}} \tag{2}$$

where ρ is the correlation coefficient, $Z_{i,1}$ is the baseline impedance data and $Z_{i,2}$ is the compared impedance data at frequency i, Z_1 and Z_2 are the means of the signals and the terms are the standard deviations. The feature examined in this study is $(1 - \rho)$, in order to ensure that, with increasing damage or change in structural integrity, the metric values also increase. Therefore, a damage metric value of zero, when compared to a baseline measurement, corresponds to perfect correlation. Perfect correlation between a given measurement and a baseline measurement, in turn, means that there is no damage present for that given measurement. A greater damage metric value means that a certain degree of dissimilarity, with respect to a baseline measurement, is present in a particular measurement. In addition, an increase in the value of the damage metric corresponds to an increase in this dissimilarity.

Figure 16 illustrates the value corresponding to $(1 - \rho)$, in which damage shows up with an increased value in damage metric. The first five measurements are made when no damage is present (i.e. baseline conditions). Tests 6 and 7 correspond to Damage A, and tests 8 and 9 correspond to Damage B. The damage metric chart is constructed after each measurement has been taken in order to give some indication of the conditions of the structure through comparison with a reference measurement. As can be seen in the figure, the baselines are repeatable, and when damage is introduced, there is an increase in the damage metric values. This correlation chart provides a quick insight into the extent of damage and provides a quantitative comparison between different data sets. Although the impedance method cannot precisely predict the exact nature and size of the damage, the method provides somewhat quantitative information about the condition of a structure by showing an increasing damage metric with increased severity of damage.

An attempt is also made to use the Lamb wave technique to locate the connection-type damage. But, the changes in Lamb wave propagations, particularly in the reflected wave from the clamped joint, were not clearly identifiable because, even after loosening the bolt, almost the same amount of waves (before and after the induced damage) are reflected from the end of the plate and holes (used for bolt connections). It should also be noted that the damage localization was somewhat difficult because of the relative small size and low damping present in the plate. The impedance responses from P1 and P3 show almost the same sensitivity as that of P2.

4. Discussion

The combined use of PZT patches for identifying structural damage has been presented. While the method shows great potential, certain issues must be addressed to handle real-world applications. The damage considered in this study (simulated crack), for implementation of the Lamb wave method on the cantilever aluminum plate, is not realistic and the performance of the proposed method must be verified with real damage. The use of wavelet analysis, instead of using the time-frequency analysis, will certainly provide advantages for this method because there is a tradeoff between time and frequency resolution in the time-frequency analysis. In addition, the threshold limit should be well established to properly classify the arrival of the reflected waves for the pulse-echo analysis. In the Lamb wave study, by mixing the use of MFC and PZT patches, the threshold limits were established for each and every PZT/MFC combination, which is quite problematical if one has a large number of sensors/actuators. Furthermore, the presence of the boundary-reflected wave makes the pulse-echo analysis quite complicated and the optimization of sensor/actuator deployment must be addressed. Finally, the automated process in signal processing for more complex geometry should be developed. All of the issues mentioned above are currently being investigated.

5. Conclusions

An integrated approach for identifying structural damage based on the use of piezoelectric materials has been presented. PZT wafers are used to actuate/sense the dynamic response of the structure with the Lamb wave propagations and impedance methods. As illustrated in the examples presented in this research, the impedance measurements can be made using the same PZT actuators/sensors used for Lamb wave propagations. For the Lamb wave propagations, both wave attenuation and reflection information are utilized to detect and locate simulated through-cracks in the structure. The impedance methods are used to detect connection-type damage, in which the wave propagation method is less sensitive. The proposed method was verified with a series of experiments. Several issues are outlined that can be used as a guideline for future investigations.

Acknowledgments

References

[1] S.S. Kessler, S.M. Spearing and C. Soutis, Damage Detection in Composite Materials using Lamb Wave Methods, *Smart Materials and Structures* **11** (2002), 269–278.

[2] J.B. Ihn and F.K. Chang, Detection and monitoring of hidden fatigue crack growth using a built-in piezoelectric sensor/actuator network: II. Validation using riveted joints and repair patches, *Smart Materials and Structures* **13** (2004), 621–630.

[3] G. Park, H. Sohn, C.R. Farrar and D.J. Inman, Overview of Piezoelectric Impedance-based Health Monitoring and Path Forward, *The Shock and Vibration Digest* **35** (2003), 451–463.

[4] F.P. Sun, Z. Chaudry, C. Liang and C.A. Rodgers, Truss Structure Integrity Identification Using PZT Sensor-Actuator, *Journal of Intelligent Material Systems & Structures* **6** (1995), 134–139.

[5] G. Park, H.H. Cudney and D.J. Inman, Impedance-based Health Monitoring of Civil Structural Components, *ASCE Journal of Infrastructure Systems* **6** (2000), 153–160.

[6] V. Giurgiutiu, A. Zagrai and J.J. Bao, Piezoelectric Wafer Embedded Active Sensors for Aging Aircraft Structural Health Monitoring, *International Journal of Structural Health Monitoring* **1** (2002), 41–61.

[7] V. Giurgiutiu, A. Zagrai and J.J. Bao, Damage Identification in Aging Aircraft Structures with Piezoelectric Wafer Active Sensors, *Journal of Intelligent Material Systems and Structures* **15** (2004), 673–688.

[8] S. Bhalla and C.K. Soh, Structural Impedance-based Damage Diagnosis by Piezo-Transducers, *Earthquake Engineering & Structural Dynamics* **32** (2003), 1897–1916.

[9] S. Bhalla and C.K. Soh, High Frequency Piezoelectric Signatures for Diagnosis of Seismic/Blast Induced Structural Damages, *NDT&E International* **37** (2004), 23–33.

[10] G. Park, H. Cudney and D.J. Inman, An Integrated Health Monitoring Technique Using Structural Impedance Sensors, *Journal of Intelligent Material Systems and Structures* **11** (2000), 448–455.

[11] A. Naidu and C.K. Soh, Damage Severity and Propagation Characterization with Admittance Signatures of Piezo Transducers, *Smart Mateirlas and Structures* **13** (2004), 393–403.

[12] N. Bourasseau, E. Moulin, C. Delebarre and P. Bonniau, Radome Health Monitoring with Lamb Waves: Experimental Approach, *NDT&E International* **33** (2000), 393–400.

[13] H. Sohn, G. Park, J.R. Wait, N.P. Limback and C.R. Farrar, Wavelet-based Signal Processing for Detecting Delamination in Composite Plates, *Smart Materials and Structures* **13** (2004), 153–160.

[14] M. Lemistre and D. Balageas, Structural Health Monitoring System based on Diffracted Lamb Wave Analysis by Multiresolution Processing, *Smart Materials and Structures* **10** (2001), 504–511.

[15] D.E. Adams and C.R. Farrar, Identifying Linear and Nonlinear Damage Using Frequency Domain ARX Models, *International Journal of Structural Health Monitoring* **1** (2002), 185–201.

[16] J.M. Nichols, M.D. Todd and J.R. Wait, Using State Space Predictive Modeling with Chaotic Interrogation in Detecting Joint Preload Loss in a Frame Structure Experiment, *Smart Materials and Structures* **12** (2003), 580–601.

[17] J.B. Han, J.C. Cheng, T.H. Wang and Y. Bertelot, Mode analysis of laser generated transient ultrasonic Lamb waveforms in composite plate by wavelet transform, *Material Evaluation* **57** (1999), 837–840.